CTPS1 inhibition synergizes with replication stress signaling inhibition in *MYC*-amplified Group 3 medulloblastoma

Matthew R Hathaway[1], Katherine E Gadek[1], Hawa L Jagana[1], Isabella C Terrones[1], John M Hemenway[1], Aya Miyaki[1], Ashmitha Rajendran[1,2], Michael Meechan[1], Leonel Elena-Sanchez[1], Nicholas A Vitanza[1,3,4,8], Barbara S Slusher[5,6], Siobhan S Pattwell[1,3,7], Myron K Evans II[1,3,7,8]*

[1] Ben Towne Center for Childhood Cancer Research, Seattle Children's Research Institute, Seattle, WA, USA
[2] Biomedical Informatics and Medical Education Graduate Program, University of Washington, Seattle, WA, USA
[3] Department of Pediatrics, University of Washington School of Medicine, Seattle, WA, USA
[4] Clinical Research Division, Fred Hutchinson Cancer Center, Seattle, WA, USA
[5] Johns Hopkins Drug Discovery, Baltimore, MD, USA
[6] Department of Neurology, The Johns Hopkins University School of Medicine, Baltimore, MD, USA
[7] Human Biology Division, Fred Hutchinson Cancer Center, Seattle, WA, USA
[8] Department of Laboratory Medicine and Pathology, University of Washington School of Medicine, Seattle, WA, USA

* Address correspondence to:
Myron K Evans II, Ph.D.
Ben Towne Center for Childhood Cancer Research
1920 Terry Avenue
Seattle, WA 98101
Telephone: +1 206-884-4363
Email: myron.evansii@seattlechildrens.org

Keywords: CTPS1; medulloblastoma; MYC; glutamine; CHK1

Financial support: National Cancer Institute of the National Institutes of Health under Award Numbers K22CA262343 (MKE) and K22CA258953 (SSP), Kate Amato Foundation (MKE), Steven Higgins Brain Tumor Research Fund (MKE), Unravel Pediatric Cancer (MKE), the Pediatric Brain Tumor Research Fund of Seattle Children's (MKE),

Seattle Children's Guild Association, and UW/FHCC/SCH Cancer Center Support Grant (P30CA015704).

Conflict of Interest

Author B.S.S. is an inventor of patent applications filed by Johns Hopkins Technology Ventures covering novel glutamine antagonists, including JHU083 and JHU395, and their utility which has been licensed to Dracen Pharmaceuticals. B.S.S. is also a co-founder and prior consultant for Dracen Pharmaceuticals. This arrangement has been reviewed and approved by Johns Hopkins University following their respective conflicts of interest policies.

N.A.V. serves as the scientific advisory board chair for BrainChild Bio, Inc. and is an inventor on issued and pending patents related to CAR T cell therapies. This arrangement has been reviewed and approved by Seattle Children's Research Institute following their respective conflicts of interest policies.

Abstract

MYC-driven medulloblastomas (MBs) represent the most aggressive and deadly subgroup of MB, the most common malignant pediatric brain tumor. Direct targeting of MYC itself remains an unmet clinical need, therefore focusing on vulnerabilities driven by MYC may be a viable option for novel therapeutic interventions. Using whole-genome CRISPR screening, we identified the *de novo* pyrimidine synthesis enzyme CTP synthase (*CTPS1*) as a strong dependency in *MYC*-driven MB. CTPS1 is the final and rate-limiting step in the *de novo* pyrimidine synthesis pathway. Targeted inhibition of CTPS1 leads to decreased tumor cell proliferation and markedly reduces MYC expression in G3 MB models. Mechanistically, we demonstrate that single agent CTPS1 inhibition activates the replication stress signaling pathway mediated by ATM-CHK2 and ATR-CHK1. Blockade of CHK1 kinase activity increases sensitivity to CTPS1 inhibition and significantly impedes heterotopic MB tumor growth. CTPS1 enzymatic activity requires the amino acid glutamine, therefore we inhibited CTPS1 using the glutamine antagonists, JHU083 and JHU395. These compounds are prodrugs of 6-diazo-5-oxo-L-norleucine (DON) which were developed to exhibit better tumor targeting and enhanced blood-brain barrier penetrability. Combining JHU083 and CHK1 inhibition demonstrates potent synergy against patient-derived MB xenografts *in vivo*. Our findings strongly suggest that combining *de novo* pyrimidine synthesis and ATR-CHK1 inhibitors is a promising treatment for *MYC*-driven MBs.

74 **Key Points**

75 - *CTPS1* is a unique vulnerability in MYC-driven medulloblastoma
76 - CTPS1 inhibition activates the ATR-CHK1 replication stress response pathway
77 for cell survival
78 - Blockade of CTPS1 enzymatic activity synergizes with CHK1 inhibition *in vitro*
79 and *in vivo*

80 **Importance of the Study**

81 MYC hyperactivation in tumors drives multiple anabolic processes which contribute to
82 tumor proliferation and aggressiveness in patients. We show that targeting *de novo*
83 pyrimidine synthesis (via CTPS1) limits tumor growth and targets MYC itself through a
84 feedback mechanism. CTPS1 inhibition potently combines with CHK1 blockade and
85 enhances disease control in both heterotopic and orthotopic models of medulloblastoma
86 (MB). Our results support the clinical evaluation of combined CTPS1 and CHK1
87 inhibition in patients with *MYC*-driven MB.

Introduction

Despite being the second most common oncological diagnosis, central nervous system tumors are the leading cause of cancer-related mortality in children[1]. Medulloblastoma (MB), the most common malignant pediatric brain tumor, exhibits a complex genomic landscape with diverse molecular subgroups which significantly impact clinical outcomes[2]. Recent advances in genomic, epigenomic, and proteomic profiling have identified four subgroups of MB: WNT, sonic hedgehog (SHH), Group 3, and Group 4. Patients with Group 3 MB account for ~25-30% of all diagnosed cases and have the poorest overall survival of all groups[2].

Dysregulation of the proto-oncogene MYC is a hallmark of G3 MB, with patients exhibiting recurrent gene amplification and genomic fusions[3] or high MYC activity due to increased protein stability[4]. Despite our understanding of MYC as a critical oncogene[5], no direct targeted agents have been tested clinically in pediatric patients. This has motivated the study of synthetic lethality approaches, targeting vulnerabilities specifically driven by MYC hyperactivation[6].

MYC supports cancer cell proliferation through numerous mechanisms, including rewiring of cellular metabolism, by modulating anabolic processes to sustain the heightened demands of rapidly dividing cells. Oncogenic MYC drives the upregulation of key enzymes crucial to nucleotide biosynthesis, ensuring a robust supply of purine and pyrimidine precursors needed for rapid tumor cell proliferation[7]. Simultaneously, MYC promotes metabolic rewiring of glycolysis and the pentose phosphate pathway (PPP), channeling resources toward nucleotide synthesis[7]. This dynamic interplay is a characteristic feature of G3 MB[8]. Further, it underscores the significance of MYC in

111 tailoring cellular metabolism to meet the unique demands of oncogenesis, unveiling
112 potential vulnerabilities that could be harnessed for targeted therapeutic interventions.
113 Inhibition of nucleotide synthesis and metabolism effectively induces cell death and is
114 commonly exploited by various chemotherapeutics sometimes used in the treatment of
115 MB[9,10]. However, these treatments commonly yield unwanted side effects in patients,
116 suggesting that targeting tumor specific metabolism pathways could alleviate negative
117 sequelae. CTP synthase 1 (CTPS1), the rate limiting enzyme in the *de novo* synthesis of
118 the nucleotide CTP, is one such metabolic target[11,12]. CTPS1 has previously been shown
119 as a vulnerability in various adult solid and hematologic tumors[13-16] and a small molecule
120 inhibitor of CTPS1 is currently in clinical trials (NCT05463263). Further, a recent paper
121 linked MYC expression to CTPS1 inhibitor sensitivity, demonstrating synthetic lethality in
122 colorectal cancer[17]. Low on-target, off-tumor toxicity of this molecule (and similar
123 compounds) is most likely due to significant compensation by the homolog CTPS2 in most
124 tissues, excluding the lymphoid compartment post-infection[18,19].
125 In this study, using functional genomics and small molecule inhibition, we characterize
126 CTPS1 as a targetable vulnerability in G3 MB and identify MYC-amplified MB as
127 exquisitely dependent on *de novo* pyrimidine but not purine synthesis. Unlike in
128 hematological malignancies where CTPS1 inhibition alone significantly inhibits growth
129 and increases apoptosis[13,16], we observe limited cytotoxicity as a single agent in G3 MB.
130 We demonstrate that inhibition of CTPS1 in G3 MB activates the ATR-CHK1 replication
131 stress response, enhancing cell survival; dual antagonism of *de novo* pyrimidine
132 synthesis and CHK1 synergizes *in vitro* and *in vivo*. Finally, we demonstrate that a blood-
133 brain barrier (BBB) penetrant inhibitor of nucleotide biosynthesis combines with CHK1

134 inhibition increasing survival in an orthotopic model of MB. Our findings identify CTPS1
135 as a novel target and demonstrate that this combinatorial approach may be a valid option
136 to move forward clinically for patients with G3 MB.

137 **Results**

138 **CTPS1 and the *de novo* pyrimidine synthesis pathway are dependencies in Group**
139 **3 medulloblastoma**

140 Functional genomics screens allow for unbiased identification of potentially druggable
141 vulnerabilities in tumors and have been utilized to guide pre-clinical work and clinical trials
142 in both adult and pediatric oncology. To evaluate dependencies specific to Group 3
143 medulloblastoma (MB), we first explored the Pediatric Cancer Dependency Map
144 (DepMap)[20]. Our analysis of 4 well-characterized G3 MB cell lines (D283, D341, D425,
145 and D458) versus all other pediatric entities, revealed CTP synthase 1 (*CTPS1*) as the
146 third-strongest dependency (defined by a negative CHRONOS score, **Figure 1A**).
147 Comparing G3 MB to only pediatric (peds) central nervous system (CNS) tumors still
148 reveals a strong dependency on *CTPS1* (**Figure S1A**), suggesting a specific function in
149 *MYC*-amplified MB. CTPS1 is the rate limiting enzyme responsible for the glutamine-
150 dependent conversion of uridine triphosphate (UTP) to cytidine triphosphate (CTP), an
151 essential step of the *de novo* pyrimidine synthesis pathway[12] (**Figure 1B**). Further
152 analysis revealed significant dependencies on other enzymes in the *de novo* pyrimidine
153 synthesis pathway including carbamoyl-phosphate synthetase 2, aspartate
154 transcarbamylase, and dihydroorotase (*CAD*), uridine monophosphate synthase (UMPS),
155 and dihydroorotate dehydrogenase (*DHODH*) (**Figure 1C,** G3 MB vs. all peds, **S1B**
156 G3MB vs. peds CNS). UMP-CMP kinase (*CMPK1*) scores as a vulnerability however, no
157 difference is seen when compared to other pediatric tumors. This is further validated by
158 a recent publication which revealed DHODH as a druggable target by CRISPR screening
159 in another G3 MB cell line (SUMB002)[21]. Mining of CRISPR screening data in two fetal

160 neural stem cell (NSC) lines[22] shows no dependency on *CTPS1* or other *de novo*
161 pyrimidine synthesis enzyme genes (**Figure S1C**). Interestingly, neither disruption of
162 *CTPS2* (**Figure 1C, S1B**) or genes in the salvage pathway (**Figure S1D**) had any effect
163 on cell growth, suggesting a strong, non-redundant role for *CTPS1* in G3 MB.
164

165 **Higher *CTPS1* expression is associated with disease advancement and poor**
166 **prognosis in MB**

167 Using a batch-normalized bulk RNA-seq resource (GSE124814)[23] comprised of 1350 MB
168 samples and 291 normal cerebellum revealed increased *CTPS1* expression in tumors
169 compared to normal cerebella (**Figure 1D**). Subgroup analysis uncovered the highest
170 average expression of *CTPS1* in G3 tumors in two independent datasets ($p<0.05$
171 G3vs.G4 and G3vs.SHH, **Figure 1E-F**). Analysis of a third dataset (GSE85217)[24] showed
172 a strong correlation between *MYC* and *CTPS1* expression in G3 MB tumors, with the
173 highest expression in those tumors characterized as Group3γ (**Figure 1G-H)**. *CTPS1*
174 expression also correlates with metastatic status of patients at time of diagnosis (**Figure**
175 **1I**), further demonstrating association with aggressive characteristics. We validated these
176 RNA-seq findings in a complementary proteomic dataset[4]. In this data, G3 MB tumors
177 were subclassified as G3a and G3b, where G3a tumors are characterized by a MYC-
178 activated state either by gene amplification or post-translational alterations which
179 increase MYC protein stability. We demonstrate higher CTPS1 protein levels in G3a vs.
180 G3b tumors (**Figure S1E**), as well as higher expression of other components of the *de*
181 *novo* pyrimidine pathway (**Figure S1F**). Immunohistochemistry of G3 MB patient-derived
182 xenografts confirms expression of CTPS1 in tumor tissue with little expression in normal

183 mouse tissue (**Figure 1J**). Weaker or no correlations were seen with other genes in the
184 pyrimidine synthesis pathway (**Figure S1G**). A correlation between *CTPS1* and *CCNB1*,
185 a key regulator of cell cycle progression and a proposed risk stratification gene[25], was
186 also noted (**Figure S1H**). Consistent with this, higher *CTPS1* expression was associated
187 with worse overall survival in all MB patients (**Figure 1K**) and in G3 MB patients with high
188 MYC expression (**Figure 1L**). Of the other *de novo* pyrimidine synthesis pathway
189 enzymes, only *DHODH* and *UMPS* expression correlated with poor survival in G3 MB
190 patients (**Figure S1I**).
191
192 **Targeting CTPS1 reduces MB cell proliferation *in vitro***
193 Based on the significant attenuation of growth using CRISPR-Cas9 targeting of *CTPS1*,
194 we targeted *CTPS1* using shRNA. After selection with puromycin, sphere formation was
195 assessed and cell proliferation measured by BrdU incorporation. In two different G3 MB
196 cell lines, cells exhibited decreased sphere forming capacity (**Figure 2A-B**), and
197 diminished proliferation concurrent with downregulation of *CTPS1* expression (**Figure**
198 **2C**). Despite significant growth inhibition *in vitro*, animals implanted with sh*CTPS1* cells
199 showed limited survival benefit compared to control shRNA implanted animals. HD-MB03
200 sh*CTPS1* tumors retained CTPS1 expression suggesting a negative selection for cells
201 with *CTPS1* knockdown *in vivo*. We next employed treatment with 3-Deazauridine (DAU)
202 which is a structural analog of uridine that competitively inhibits the synthesis of CTP by
203 both CTPS1 and CTPS2[26]. DAU treatment caused a dose-dependent decrease in cell
204 proliferation across a panel of G3 MB cell lines (**Figure 2D**). This inhibition could be
205 reversed by supplementation of either uridine or cytidine, but not adenosine or guanosine

206 (**Figure 2E**). Similar to previously published data[14,27], CTPS1 pharmacological inhibition
207 resulted in S-phase blockade with decreased cells in G_0-G_1, which was reversed by
208 addition of cytidine or uridine (**Figure 2F, S2A**). Furthermore, DAU treatment also
209 decreased MYC expression in tumor lines similar to previous reports with DHODH
210 inhibition in G3 MB[21] (**Figure 2G**).
211
212 **G3 MB cells are dependent on *de novo* pyrimidine but not *de novo* purine synthesis**
213 Previous work in other tumor types has revealed that MYC regulates both pyrimidine and
214 purine biosynthesis through direct regulation of multiple enzyme-encoding genes in both
215 pathways[7]. Analysis of previously published ChIP-seq data from two human G3 MB
216 tumors demonstrates significant MYC binding at the *CTPS1* promoter, with lower binding
217 at the *CTPS2* promoter correlating with gene expression[28] (**Figure S3A,B**). Analysis of
218 the same dataset from **Fig 1D**. revealed strong correlation between *MYC* and numerous
219 genes encoding enzymes in the *de novo* purine synthesis pathway (**Figure S3C**).
220 Exploration of DepMap data revealed that while some genes in the pathway scored as
221 dependencies, they were no different than pediatric CNS tumors (**Figure S3D**). The only
222 purine related enzyme that scores is thymidylate synthetase (TYMS), a catabolic one-
223 carbon metabolism enzyme that has an indirect effect on purine by driving thymidine
224 synthesis from dUMP salvage (**Figure S3E**). This correlates with activity of TYMS
225 inhibitors pemetrexed and 5-fluorouracil[29,30] and suggests the possibility of recently
226 developed novel inhibitors for future pre-clinical modeling[31,32].
227 To further clarify that inhibition of pyrimidine but not purine synthesis was antagonistic to
228 growth of G3 MB cells, we treated both Med-2112FHTC and Med-411FHTC with

229 lometrexol (LTX), an inhibitor of the purine biosynthetic enzyme glycinamide
230 ribonucleotide formyltransferase (GARFT). We observed no effect on cell fitness after
231 treatment with LTX, similar to previous reports in IDH-mutant glioma and pediatric diffuse
232 midline glioma[33] (**Figure S3F**).
233

234 **CTPS1 inhibition alone is cytostatic but combines with CHK1 inhibition**

235 Western blot analysis of cells treated with DAU revealed little change in PARP cleavage,
236 a classic marker of apoptosis, at doses up to 5μM suggesting a cytostatic mechanism
237 rather than cytotoxicity (**Figure 3A**). Diehl et.al. recently published that nucleotide
238 imbalance, caused by targeting pyrimidine and/or purine enzymes, activates replication
239 stress signaling sensed by the ATR and ATM kinases[27]. These kinases sense both single-
240 and double- stranded breaks and phosphorylate CHK1 and CHK2, respectively, which
241 mediate survival and recovery of cells. We observed increased phosphorylation of both
242 CHK1 and CHK2 after treatment with DAU (**Figure 3B**). We then combined targeting of
243 CTPS1 with the potent CHK1/2 inhibitor prexasertib, which previously showed efficacy in
244 G3 MB cells[34]. Combining sublethal doses of prexasertib (**Figure S4A**) led to a dose-
245 dependent decrease in the IC_{50} of DAU in both HD-MB03 and Med-411FHTC cells
246 (**Figure 3C and D**). **Table 1** lists synergy scores as calculated by multiple reference
247 models[35] which revealed potent synergy between CTPS1 and CHK1/2 inhibition in G3
248 MB. This combination also led to apoptosis (**Figure 3C, inset** – cleaved PARP) and
249 significant DNA damage (measured by pH2AX) (**Figure 3E-F**). Prexasertib treatment also
250 synergized with BRQ, suggesting that CHK1 inhibition may broadly combine with
251 antagonism of *de novo* pyrimidine synthesis in G3 MB (**Figure S4B**). Utilizing a

252 heterotopic xenograft model of G3 MB in athymic nude mice, we assessed the efficacy of
253 combining DAU and prexasertib on tumor growth (**Figure 3G**). While single agent
254 targeting of either CTPS1 or CHK1 led to delays in tumor growth, the combination of DAU
255 and prexasertib synergized and completely abrogated growth in this model (**Figure 3H**).
256 Immunohistochemical analysis revealed decreased Ki67 corroborating our doubling time
257 findings (**Figure 3I**). Phosphorylation of H2AX was also elevated in combination treated
258 animals. Western blots revealed significant cleavage of PARP in our combination
259 treatment and sustained phosphorylation of CHK1/CHK2 (S345/S516) in combination
260 treatments (**Figure 3J**). We also noted decreased phosphorylation of the CHK1 target
261 CDC2 (Y15) in some combination treatment mice as well.
262

263 **Targeted glutamine antagonism combines with CHK1 inhibition in orthotopic**
264 **models**

265 While our *in vitro* and *in vivo* data with DAU are striking, there is only one reference to
266 blood-brain barrier penetration of this compound in humans[36]. This was evaluated in a
267 handful of patients with intracerebral tumors which commonly have abnormally leaky
268 vasculature[37]. MBs, apart from the WNT subgroup, are characterized to have a fully intact
269 BBB which modulates response to BBB-impermeable drugs[38]. The combination of these
270 make DAU an unlikely candidate for G3 MB therapeutic development. CTPS enzymatic
271 activity requires the amino acid glutamine as well as ATP to produce CTP[39]. Glutamine is
272 also required at the first step of the *de novo* synthesis pathway catalyzed by CAD (**Figure**
273 **1B**). Interestingly, the glutamine antagonist 6-diazo-5-oxo-l-norleucine (DON) was
274 previously shown to be an irreversible inhibitor of multiple nucleotide synthesis

275 enzymes[40], including CTPS1 and CAD. Single agent DON administration leads to
276 significant phosphorylation of CHK1/2 (**Figure 4A**) and cell death in G3 MB tumor cells[41].
277 We utilized two prodrugs of DON – 1) isopropyl 6-diazo-5-oxo-2-(((phenyl (pivaloyloxy)
278 methoxy) - carbonyl) amino) hexanoate (JHU395) and 2) Ethyl 2-(2-Amino-4-
279 methylpentanamido)-DON (JHU083) – which exhibit enhanced lipophilicity, brain
280 penetration, and were previously shown to target G3 MB tumor cells[41,42] (**Figure S5A**).
281 We first tested JHU083 and JHU395 as single agents in our patient-derived cell lines
282 which revealed efficacy with inter-cell line variability (**Figure 4B**). Co-administration of
283 prexasertib synergized with both JHU083 (**Figure 4C and D**) and JHU395 (**Figure 4E**
284 **and F**), decreasing the IC_{50} in multiple G3 MB tumor lines. Synergy analyses (**Table 1**)
285 revealed stronger synergism of prexasertib with JHU083 than with JHU395, so for the
286 remainder of our study we used the combination of JHU083+prexasertib. Combining
287 JHU083 and prexasertib led to significant accumulation of DNA damage (**Figure 4G-H**)
288 similar to DAU+prexasertib. Previous work demonstrated significant BBB penetration and
289 tumor accumulation of both JHU083[42] and prexasertib[43] in G3 MB tumor bearing mice,
290 therefore we tested single agents and combinations after orthotopic implantation of
291 luciferase-expressing G3 MB cells. After confirmation of tumor growth by IVIS imaging,
292 mice were randomized to one of four groups and treated with JHU083 alone or in
293 combination with prexasertib (**Figure 4I**). While single agent administration had limited
294 effect on tumor growth or animal survival, the combination of JHU083 and prexasertib
295 significantly extended the median survival in animals implanted with either HD-MB03
296 (**Figure 4J, S5B**) or Med-411FHTC (**Figure 4K, S5C**). Further, this combination as well
297 as our DAU+prexasertib combination had limited systemic toxicities as measured by

298 weight loss in animals (**Figure S5D,E**). Western immunoblot analysis of tumors revealed
299 increased phospho-CHK1/2 and phospho-CDC2 in JHU083 single agent treated tumors.
300 Combination treatment led to a blockade of CHK1/2 and CDC2 phosphorylation as well
301 as a decrease in proliferation as measured by PCNA (**Figure 4L**).

302 **Discussion**

303 Herein, we report a dependency on *CTPS1* in *MYC*-amplified MBs when compared to
304 other pediatric malignancies. Interrogation of patient data revealed high expression of
305 *CTPS1* in tumors compared to normal brain (cerebellum/upper rhombic lip) with *MYC*-
306 amplified G3γ tumors displaying the highest expression. This was confirmed using
307 recently published proteomics data which correlates CTPS1 with G3a tumors,
308 characterized by increased MYC expression and activity[4]. Consistent with these findings,
309 *CTPS1* expression correlates with poor survival in *MYC* high patients. CTPS1, along with
310 its homolog CTPS2, catalyze the rate limiting step of the *de novo* pyrimidine biosynthesis
311 pathway. Interestingly, *MYC*-amplified MB tumors do not show a dependency on CTPS2,
312 which also shows no correlation with survival. This is consistent with previous reports that
313 demonstrate differential activity of the two enzymes, despite ~70% protein sequence
314 homology[44]. Further analysis revealed vulnerabilities to deletion of other members of the
315 *de novo* pyrimidine biosynthesis pathway, confirming previous reports of altered
316 pyrimidine metabolism in MYC-amplified MB[21], and more broadly across a number of
317 other brain tumor types[33]. Furthermore, recent work in a chemotherapy-resistant model
318 of MB revealed upregulation of pyrimidine metabolic processes in resistant tumors[45],
319 suggesting utility of CTPS1 targeting in both upfront and recurrence settings.

320 Using shRNAs and a small molecule inhibitor of CTPS1 (3-deazuridine, DAU) we
321 demonstrate that single agent targeting of CTPS1 leads to cell cycle arrest and decreased
322 proliferation which can be rescued by addition of exogenous pyrimidine nucleosides *in*
323 *vitro*. This targeting of CTPS1 also leads to a decrease in MYC expression which may
324 further impact tumor growth. Interestingly, germline mutations in *CTPS1* lead to no overt

325 phenotypes outside of the hematopoietic system, suggesting that inhibition may deliver
326 potent on-target effects in tumors while limiting deleterious side effects in patients[18,19].
327 This is highlighted by single agent efficacy of DAU in our flank model with no significant
328 weight loss observed. Mechanistically, amplified or hyperactive MYC in G3 MB induces
329 expression of CTPS1 required to synthesize nucleosides to maintain replicative capacity
330 of tumors. Inhibition of CTPS1 limits the pool of CTP available for replication[9], leading to
331 activation of the replication stress response pathway mediated by ATR-CHK1/ATM-CHK2
332 and subsequent cell cycle and proliferation arrest. Combined targeting of CTPS1 and the
333 replication stress pathway forces cells to continue through the cell cycle, accumulating
334 significant DNA damage and undergoing apoptosis (**Figure 5**).
335 This phenomenon has been observed in other tumor and normal cell types wherein
336 combining nucleotide depletion with ATR/ATM inhibitors leads to cell death[14,17,27]. We
337 demonstrate significant synergy between the CHK1 inhibitor, prexasertib, and DAU both
338 *in vitro* and *in vivo*. Further, we also demonstrate that the DHODH inhibitor, brequinar,
339 also synergizes with prexasertib suggesting the utility of dual *de novo* pyrimidine
340 synthesis and replication stress signaling inhibition in treatment of *MYC*-amplified MB.
341 Identification of this combination may further enhance the clinical utility of a DHODH
342 inhibitor from Bayer which shows potent BBB penetration, but whose clinical development
343 was halted due to single agent inactivity (NCT03404726).
344 Excitingly, CTPS1 inhibitors have recently entered clinical development (NCT05463263)
345 for hematological malignancies; however, blood-brain barrier (BBB) penetrance has not
346 been assessed. This compound (STP938) mimics CTP and acts an allosteric inhibitor of
347 enzymatic activity; impeding CTPS1 binding to UTP. CTPS1 also has a glutamine

348 amidotransferase domain which hydrolyzes glutamine to ammonia which is required for
349 catalysis of 4-phosphoryl UTP to CTP. Previous work identified that the glutamine
350 antagonist 6-Diazo-5-oxo-L-norleucine (DON) binds to this domain, as well as other
351 glutamine utilizing enzymes, to inhibit covalent binding of glutamine[40]. We observed a
352 similar activation of CHK1/2 when cells were treated with DON as with DAU. While DON
353 does accumulate in mouse models of brain tumors, previous clinical trials were
354 unsuccessful due to dose-limiting toxicities[46]. We utilized two DON prodrugs, JHU083 and
355 JHU395, with enhanced BBB penetrability and tumor-targeting, leading to reduced toxic
356 side effects[47,48]. These inhibitors combine strongly with CHK1 inhibition *in vitro*, with the
357 combination of JHU083 and prexasertib showing significant synergy. We tested this
358 combination *in vivo* and noted increased survival, decreased proliferation, and increased
359 apoptosis, and limited weight loss despite prolonged combination treatment. While our
360 studies are done in immune-deficient models, recent studies have identified immune
361 modulatory activity of JHU083[49,50] which may bolster effects of this drug in immune-
362 competent mouse models and patients. Together, the data presented herein identify a
363 targeted, combinatorial approach for the treatment of *MYC*-amplified MB patients who
364 currently have the least favorable outcomes.

365 **Methods**

366 **Cell culture**

367 Patient derived medulloblastoma cell lines (Med-411FHTC and Med-2112FHTC, a gift
368 from J. Olson) were grown in NeuroCult NS-A Basal medium (Stemcell Technologies,
369 05750) with Neurocult NS-A Proliferation Supplement (Stemcell Technologies, 05753),
370 and 1% Penicillin/Streptomycin (Sigma-Aldrich, P4333). HD-MB03 (obtained from T.
371 Milde) and MB004 (a gift from P. Bandopadhayay) cell lines were grown in Gibco
372 Neurobasal medium (Gibco, 21-103-049) with 2% B27 Supplement (Gibco, 12587010),
373 1% N2 Supplement (Gibco, 21103049), 1% Glutamine (Gibco, 25030-81), 1%
374 Penicillin/Streptomycin (Sigma-Aldrich, P4333), and 1μg/mL Heparin (Stemcell
375 Technologies, 07980). All cell lines were grown as spheroids and media supplemented
376 with 0.2μg/mL each Human Epidermal Growth Factor Protein (Sino Biological, 10605-
377 HNAE-1) and Human Recombinant bFGF/FGF2 Protein (Sino Biological, 10014-HNAE-
378 1). HEK293T were obtained from American Type Culture collection and maintained in
379 DMEM (Gibco) with L-glutamine (Fisher Sci.), 10% fetal bovine serum (Fisher Sci.), 1%
380 L-Glutamine, and 1% Penicillin/Streptomycin (Sigma-Aldrich, P4333). All cells were
381 grown at 37°C and 5% CO_2.

382 **Drugs and small molecules**

383 3-Deazuridine (DAU) was obtained from Santa Cruz Biotechnology (394445) or Cayman
384 Chemical Company (23125). JHU395 and JHU083 were a gift from Barbara Slusher
385 (Johns Hopkins). Prexasertib mesylate (206787) and Prexasertib HCl (206989) were
386 procured from MedKoo Biosciences. Brequinar was procured from SelleckChem (S6626)
387 and Lometrexol from Cayman Chemical Company (18049). 6-diazo-5-oxo-L-nor-Leucine

388 (DON) was procured from Cayman Chemical Company (17580). Guanosine (S2439),
389 Adenosine (S1647), Cytidine (S2053), and Uridine (S2029) were procured from
390 SelleckChem. For *in vitro* use, drugs were reconstituted in DMSO (Millipore Sigma,
391 D2438).

392 **Proliferation measurements**

393 For Cell Titer Glo, cells were treated with serial concentrations of Prexasertib (0-20nM),
394 DAU (0-30nM), JHU083 (0-20μM), JHU395 (0-20μM), Lometrexol (0-180nM), and
395 Brequinar (0-180nM) or indicated combinations, then incubated for 72 hours. Proliferation
396 was assessed with CellTiter-Glo 2.0 (Promega, G9242) according to manufacturer
397 instructions and quantified using a Spectramax iD5. For BrdU assessment, cells
398 (untreated or treated as indicated) were incubated with 10μM BrdU (ThermoFisher,
399 B5002) for 1hr. After incubation, cells were rinsed with 1X PBS (Cytiva, BSS-PBS-1X6),
400 fixed in ice-cold 70% ethanol, and stored at -20°C. Fixed cells were washed with DPBS
401 and incubated in 2N HCl/0.5% Triton X-100 for 20 min. Cells were stained with anti-BrdU
402 FITC antibody (BioLegend, 364104) for 1 hour and analyzed on a BD Accuri C6 and
403 FlowJo (BD Biosciences).

404 **Cell cycle measurement**

405 For cell cycle measurement, cells were treated as indicated and fixed in ice-cold 70%
406 ethanol after PBS wash. FxCycle PI/RNase Staining Solution (ThermoFisher, F10797)
407 was added to cells as per manufacturer instruction. Analysis was performed on a BD
408 Accuri C6 and cell cycle analysis performed in FlowJo (BD Biosciences).

409 **Lentiviral shRNA production**

410 Lentiviral shRNA plasmids (U6 promoter) were designed and produced by Vectorbuilder.
411 shRNA sequences were:
412 shCTPS1: GCTCTCACATTACCTCCAGAA (TRCN0000045349)
413 shCTPS2: CGCCTCACCAAGGACAATAAT (TRCN0000369478)
414 HEK293T cells were plated on a 10cm dish (Corning, 877222) until 60-70% confluent.
415 Cells were transfected with 10μg transfer plasmid (VectorBuilder), 9μg psPAX2
416 (Addgene, 12260) and 3μg pMD2.G (Addgene, 12259) using Xfect Transfection Reagent
417 (Takara, 631318) according to manufacturer instructions. After transfection, virus was
418 collected in Neurobasal media, filtered through a 0.45μm syringe filter (Globe Scientific,
419 SF-PES-4530-S) and stored at -80°C. Viral particles were added to tumorspheres with
420 8μg/mL polybrene (Millipore Sigma, TR-1003-G) overnight. Forty-eight hours post-
421 infection, puromycin (Millipore Sigma, P4512-1MLX10) was added at 1μg/mL for 14 days
422 to select for infected cells.

423 **Western immunoblotting**

424 After indicated treatments, cells were lysed in RIPA buffer (150 mM NaCl; 50 mM Tris pH
425 8.0; 1.0% IGEPAL CA-630; 0.5% sodium deoxycholate; 0.1% SDS) (Thermo Scientific,
426 PI89900) with Halt protease and phosphatase inhibitor (Thermo Scientific, PI78445). For
427 tumor tissue, tissue was homogenized using an electric homogenizer fitted with a
428 disposable pestle in RIPA buffer. Protein was quantified using Pierce 660nm Protein
429 Assay Reagent (Thermo Scientific, 22660) and immunoblotted with standard procedures.
430 Antibodies and concentrations are listed Table S1.

431 **Immunofluorescence staining**

432 FFPE sections from flank tumors were deparaffinized and rehydrated with Histoclear
433 (HS2001, Fisher) and ethanol according to manufacturer instructions. Antigen retrieval
434 was performed by pressurized retrieval in pH 6.0 citrate buffer (C9999, Millipore Sigma)
435 for 5 min on high pressure in a pressure cooker (Cuisinart CPC-600 6 Quart 1000 Watt
436 Electric Pressure Cooker). Samples were blocked in 0.1% PBS+TX-100 5% donkey
437 serum (S30-M, Millipore Sigma) for 1 hr at RT prior to staining with antibodies overnight
438 at 4C. Secondary Alexa fluor antibodies (donkey anti-488, 555 or 647; Invitrogen) were
439 diluted at 1:500 in blocking buffer for 1 hour at RT. Samples were mounted in Prolong
440 Gold with NucBlue (P36981, Fisher Scientific). All samples were imaged on a Leica DMi8
441 microscope with Thunder deconvolution software (LAS X, Leica Microsystems) and
442 quantified in ImageJ.

443 **Synergy analysis**

444 Visualization and analysis of drug combinations were performed using the SynergyFinder
445 web application (version 3.0, https://synergyfinder.fimm.fi) using viability as readout.
446 Outlier detection was on with LL4 curve fitting. Bliss, ZIP, HSA, and Loewe scores and p-
447 values were calculated as described[35].

448 **Mouse xenograft experiments**

449 All animal procedures were approved by Institutional Animal Care and Use Committee
450 (IACUC) of Seattle Children's Research Institute (Protocol #00000675). Nude female
451 mice (Jackson Laboratories, NU:J- 002019 or 007850) were procured at 5 weeks of age
452 and allowed to acclimate for at least 1 week prior to cell implantation. Luciferase-
453 expressing cells were made by transduction of single cells with pLenti CMV mCherry-

454 T2A-Luc blast (a gift from N. Vitanza) followed by hand selection of positive tumorsphere
455 colonies.

456 ***Subcutaneous implantation***

457 Patient-derived MB cells were dissociated with Accutase (AT-104, Innovative Cell
458 Technologies), resuspended in Gibco Neurobasal Medium (21103049, Fisher Scientific),
459 and injected into the flank in a 100 μL aliquot containing 1.25×10^6 cells. Mice were
460 randomly segregated into groups when tumors reached 100 mm^3 volume: vehicle,
461 Prexasertib (10mg/kg subcutaneous twice daily), 3-Deazuridine (75mg/kg
462 intraperitoneal), or combination until health-defined end points. Tumor size was measured
463 with calipers. For growth curve analysis and survival studies, mice in study cohorts were
464 sacrificed when tumors reached a max of 3000 mm^3 in total volume. The tumors were
465 excised from sacrificed mice and subjected to routine histopathological processing.

466 ***Orthotopic implantation***

467 MB tumorspheres were treated with Accutase and approximately 100,000 mCherry-
468 positive cells injected per mouse in 2μL of sterile PBS (Cytiva, BSS-PBS-1X6). For
469 surgery, mice were given buprenorphine ER for analgesia and anesthetized with a
470 ketamine/xylazine mixture. A 0.9mm burr hole was made in the right cerebellum (-1.0mm
471 AP 1.0mm ML) from lambda and a stereotactic needle dispensed the cells in two 1μL
472 injections (2.5mm and 2.0mm DV) to deliver the cells. To monitor tumor growth, mice were
473 injected with 150 mg/kg of D-luciferin (LUCK-4G, Gold Biotechnologies), and imaged
474 using the IVIS Spectrum Imaging System 15 minutes post-injection.

475 ***In vivo* drug administration**

476 JHU083 was prepared in sterile PBS without Ca and Mg (Cytiva, BSSPBS1X6) and
477 administered at a concentration of 20mg/kg via oral gavage twice weekly. Prexasertib
478 mesylate (MEDKoo Biosciences, 206787) or prexasertib HCl (MEDKoo Biosciences,
479 206989) were prepared in 10% SBE-β-CD (MedChem Express, Cat# HY-17031/CS-
480 0731) and dosed at a concentration of 10mg/kg subcutaneously twice daily. 3-
481 Deazuridine (Santa Cruz Biotechnology, 394445) was diluted in corn oil (Millipore Sigma,
482 C8267-500ML) and dosed at a concentration of 75mg/kg IP once daily.

483 **Dependency Map Analysis**

484 Dependency data (CERES score) from the Broad Institute's Pediatric Cancer
485 Dependency Map[20] was accessed from the 23Q4 data deposit (depmap.org).

486 **Patient gene expression and proteomic analyses**

487 The processed expression of indicated genes were downloaded from the *R2: Genomics*
488 *Analysis and Visualization Platform* (**http://r2.amc.nl**) for indicated data sets[3,23,24]. When
489 calculating expression differences between different groups they were considered
490 significantly different when $P < 0.05$, as calculated using the one-way analysis of variance
491 (ANOVA) test included in the R2 online software. Linear regression was used to define
492 R-values and p-values for correlation plots. For significance of differences between
493 primary and metastatic tumors, the p-value was calculated with an unpaired
494 Student *t* test. For survival analyses in Kaplan–Meier plots, we used a 5-year/60-month
495 time point as a cut-off for survival due to the potential risk of including secondary tumors.
496 The *P* value for survival curves is calculated using a log-rank test of reported patient
497 survival data as described in R2 (**https://r2.amc.nl**). Only *a priori* fixed cut-offs (median

498 or top 1/3 v bottom 2/3) were used to calculate *P* values in the Kaplan–Meyer survival
499 analysis.
500 Proteomics data was downloaded from the Medulloblastoma Data Explorer
501 (https://medullo.shinyapps.io/archer2018/). One-way ANOVA was used to determine
502 significant differences.

503 **Acknowledgements**

504 We thank the University of Washington/Fred Hutchinson Cancer Center/Seattle
505 Children's Hospital Cancer Consortium for shared resources including Flow Cytometry
506 and Cell Sorting and Research Pathology supported by NCI P30CA015704. We thank
507 Virginia Hoglund and Galen Stewart for histopathology support, Jim Olson for providing
508 PDX tissue and cell lines, Beth Lawlor for reagent support, Karuna Patil and Rajesh
509 Utamanthil for animal husbandry and veterinary support. Research reported in this
510 manuscript was funded by the National Cancer Institute of the National Institutes of
511 Health under Award Numbers K22CA262343 (MKE) and K22CA258953 (SSP), Kate
512 Amato Foundation (MKE), Steven Higgins Brain Tumor Research Fund, Unravel
513 Pediatric Cancer, the Pediatric Brain Tumor Research Fund of Seattle Children's, the
514 Run of Hope Seattle, Seattle Children's Guild Association, and UW/FHCC/SCH Cancer
515 Center Support Grant (P30CA015704).

516

517 **Author contributions**

518 **Matthew R Hathaway:** Conceptualization, Data curation, Formal analysis,
519 Investigation, Methodology, Validation, Visualization, Writing – original draft, Writing –
520 review & editing. **Katherine E Gadek:** Data curation, Formal analysis, Investigation,

Methodology, Validation, Visualization, Software, Writing – original draft, Writing – review & editing. **Hawa L Jagana:** Data curation, Writing – review & editing. **Isabella C Terrones:** Data curation, Formal analysis, Writing – review & editing. **John M Hemenway:** Data curation, Formal analysis, Writing – review & editing. **Aya Miyaki:** Data curation, Writing – review & editing. **Ashmitha Rajendran:** Investigation, Writing – review & editing. **Michael Meechan:** Data curation, Investigation, Writing – review & editing. **Leonel Elena-Sanchez:** Data curation, Investigation, Writing – review & editing. **Nicholas A. Vitanza:** Methodology, Resources, Writing – review & editing. **Barbara S Slusher:** Methodology, Resources, Writing – review & editing. **Siobhan S Pattwell:** Methodology, Resources, Writing – review & editing. **Myron K Evans II:** Conceptualization, Funding acquisition, Methodology, Project administration, Software, Supervision, Validation, Writing – original draft, Writing – review & editing.

533 **Figure Legends**

534 **Figure 1: *CTPS1* is overexpressed in medulloblastoma and is a dependency in G3**
535 **MB. a,** Volcano plot comparing CERES scores of G3 MB cell lines (D283, D425, D458,
536 D341) versus other pediatric tumor lines (n=111) in the Dependency Map using two class
537 comparison. **b,** Diagram of *de novo* pyrimidine synthesis pathway, **c,** CERES gene
538 dependency scores for pyrimidine synthesis genes in G3 MB cells (n=4) compared to
539 other pediatric cell lines (n=111) in the DepMap, 23Q4 release. **d,** Quantile normalized
540 expression of CTPS1 in normal (n=291) or primary medulloblastoma (n=1350) samples.
541 **e-f,** Log_2 normalized expression of CTPS1 in GSEs (e-GSE124814, f-
542 EGAS00001001953). Samples are separated by MB subgroup. **g,** Linear regression of
543 log_2 normalized CTPS1 and MYC expression from GSE85217 separated by subtype. **h,**
544 Log_2 normalized expression of CTPS1 in G3 MB subtypes from same samples in **g**. **i,**
545 Log_2 normalized CTPS1 expression in primary tumor samples from patients with or
546 without metastases at diagnosis from GSE85217. **j,** Immunohistochemistry of G3 patient-
547 derived xenograft tissue after orthotopic implantation in nude mice (red-CTPS1, green-
548 human nuclear antigen (hNuc), blue-DNA). Scale bar=100 μM. **k,** Kaplan-Meier survival
549 of patients diagnosed with MB separated by median expression of *CTPS1*, GSE85217. **l,**
550 Kaplan-Meier survival of *Myc*-high G3 MB patients separated by top 1/3 versus bottom
551 2/3 expression of *CTPS1*. For **k** and **l**, number of patients are shown on inset. *, $P < 0.05$;
552 **, $P < 0.01$; ***, $P < 0.001$, Data are means ± SEM.

553 **Figure 2: CTPS inhibition suppresses cell proliferation in G3 MB tumor cells. a,**
554 Representative images of HD-MB03 tumorspheres transduced with indicated shRNAs
555 72h after plating. **b,** Quantification of area of tumorspheres formed in shScramble,

556 shCTPS1.1, and shCTPS1.2 transduced HD-MB03 cells. **c,** Quantification of FACS for
557 BrdU-positive HD-MB03 and MED-411FHTC cells transduced with indicated shRNAs
558 (n=3). *Inset*, Western immunoblot analysis of CTPS1 expression in transduced cells in **a-**
559 **c** Scr= scramble, 1.1 =shCTPS1.1, 1.2= shCTPS1.2. **d,** Cell proliferation analysis of HD-
560 MB03, MB004, Med-411FHTC, and Med-2112FHTC tumorspheres treated with indicated
561 concentrations of DAU for 72h. **e,** Cell proliferation analysis of HD-MB03 and Med-
562 411FHTC tumorspheres treated with vehicle or DAU (5μM) alone or in the presence of
563 50μM cytidine, uridine, adenosine, or guanine (n=3). **f,** Cell-cycle analysis of HD-MB03
564 cells treated with the indicated concentrations of DAU alone or in the presence of cytidine
565 (C) or uridine (U) for 48h (n=3). **g,** Western immunoblot analysis of MYC expression in
566 HD-MB03 cells treated with increasing doses of DAU. *, $P < 0.05$; **, $P < 0.01$; ***, $P <$
567 0.001, Data are means ± SEM.

568 **Figure 3: CTPS1 inhibition synergizes with ATR-CHK1 blockade *in vitro* and *in vivo*.**
569 Western immunoblot for **a,** PARP and **b,** phospho-CHK1/2 in Med-411FHTC or HD-MB03
570 cells treated with vehicle, 2.5μM, or 5μM DAU for 48h. **c,** Cell proliferation analysis of
571 Med-411FHTC (left) and HD-MB03 (right) tumorspheres with increasing concentrations
572 of DAU alone or in the presence of indicated prexasertib (CHK1 inhibitor) concentrations
573 (n=3). *Inset*, Western immunoblot analysis of cleaved PARP in cells treated with
574 prexasertib alone (1.25nM), DAU alone (2.5μM), or the combination. **d,** 2D contour plots
575 of synergy (Bliss calculation) between DAU and prexasertib in Med-411FHTC (left) and
576 HD-MB03 (right) tumorspheres calculated by Synergy Finder. **e,** Immunofluorescence for
577 phospho-H2AX in D283 G3 MB cells treated as indicated. Scale bar 25 μM. **f,**
578 Quantification of images in **e** (n=5 images per condition, experiment repeated twice). **g,**

579 Pre-clinical mouse treatment protocol for data shown in **h**. **h,** left – Tumor volume of HD-
580 MB03 flank xenografts treated as indicated n=5 (vehicle) or 6 (all others). Tumor volume
581 statistics (p-value) – veh-prex: 3.9E-6, veh-combo: 3.1E-11, prex-combo: 8.7E-3. TGI:
582 tumor growth inhibition DT: doubling time; right – Quantification of tumor weights in grams
583 at Day 20 post-treatment (veh, n=2, DAU, n=3, prex, n=3, combo, n=5). **i,** Representative
584 images of immunohistochemistry for Ki-67 and phospho-H2AX in tumors at endpoint. **j,**
585 Western immunoblot for total PARP (* denotes cleaved PARP) and phospho-CHK1/2 in
586 tumors from **h,**. *, P < 0.05; **, P < 0.01; ***, P < 0.001, Data are means ± SEM.

587 **Figure 4: CTPS1 inhibition via glutamine analogs synergizes with CHK1 inhibition**
588 **in orthotopic G3 MB models. a,** Western immunoblot for phospho-CHK1/2 in Med-
589 411FHTC (left) and HD-MB03 (right) tumorspheres treated with 10μM DON. **b,** Cell
590 proliferation analysis of HD-MB03, MB004, Med-411FHTC, and Med-2112FHTC
591 tumorspheres treated with indicated concentrations of JHU083 (left) and JHU395 (right)
592 for 72h (n=3). Cell proliferation analysis and 2D contour plots of synergy (Bliss calculation)
593 for **c, d** JHU083 and **e, f** JHU395 alone or in the presence of indicated prexasertib
594 concentrations (n=3). **g,** Immunofluorescence for phospho-H2AX in D283 G3 MB cells
595 treated as indicated. Scale bar 25 μM. **h,** Quantification of images in **g** (n=5 images per
596 condition, experiment repeated twice). **i,** Pre-clinical mouse treatment protocol for data
597 shown in **j-k**. Kaplan-Meier survival of mice orthotopically implanted with **j,** HD-MB03 or
598 **k,** Med-411FHTC cells transduced with luciferase expressing construct and treated as
599 indicated. **l,** Western immunoblot for phospho-CHK1/2, phospho-CDC2, and PCNA in
600 tumors from **j-k**. *, P < 0.05; **, P < 0.01; ***, P < 0.001, Data are means ± SEM.

601 **Figure S1: Dependency, gene expression and survival data for additional de *novo***
602 **pyrimidine synthesis and salvage pathway genes in G3 MB. a,** Volcano plot
603 comparing CERES scores of G3 MB cell lines (D283, D425, D458, D341) versus other
604 pediatric CNS tumor lines (n=17) in the Dependency Map using two class comparison. **b,**
605 CERES gene dependency scores for pyrimidine synthesis genes in G3 MB cells (n=4)
606 compared to other pediatric CNS tumor lines (n=17) in the DepMap, 23Q4 release. **c**,
607 CERES scores for normal NSCs (CB660 and U5) for *de novo* pyrimidine synthesis genes
608 as well as *TOP2A* and *RPA2* (controls). **d**, CERES gene dependency scores for
609 pyrimidine salvage genes in G3 MB cells (n=4) compared to all pediatric (left, n=111) and
610 peds CNS (right, n=17). **e**, Relative CTPS1 protein expression in G3a (n=8) and G3b
611 (n=6) tumors from(ref). **f**, Heatmap of relative protein expression for other *de novo*
612 pyrimidine synthesis proteins. **g**, Linear regression of $\log_2$ normalized *MYC* and *de novo*
613 pyrimidine synthesis gene expression from GSE85217 separated by subtype. **h**, Linear
614 regression of $\log_2$ normalized *CTPS1* and *CCNB1* expression separated by G3 subtype.
615 **i**, Kaplan-Meier survival of *MYC*-high G3 MB patients separated by top 1/3 versus bottom
616 2/3 expression of indicated genes. Number of patients are shown on inset.
617 **Figure S2: DAU treatment alters cell cycle in G3 MB. a,** Cell-cycle analysis of Med-
618 411FHTC cells treated with the indicated concentrations of DAU alone or in the presence
619 of cytidine (C) or uridine (U) for 48h (n=3). *, $P < 0.05$; **, $P < 0.01$; ***, $P < 0.001$, Data
620 are means ± SEM.
621 **Figure S3: MYC drives expression of pyrimidine and purine synthesis genes, but**
622 **G3 MB cells are insensitive to purine synthesis inhibition. a,** Representative ChIP-
623 sequencing tracks for MYC in human G3 MB cells at *CTPS1* and *CTPS2* promoters. **b,**

624 Expression (transcripts per million, TPM) of *CTPS1* and *CTPS2* in tumor samples from **a**.
625 **c,** Linear regression of $\log_2$ normalized *MYC* and *de novo* purine synthesis gene
626 expression in G3 tumors. **d**, CERES gene dependency scores for *de novo* purine
627 synthesis genes in G3 MB cells (n=4) compared to peds CNS (n=17) cell lines. **e**, left -
628 CERES scores for *TYMS* in G3 MB (n=4), all peds (n=111), and peds CNS (n=17); right
629 - Linear regression of $\log_2$ normalized *MYC* and *TYMS* expression in G3 tumors. **f**, Cell
630 proliferation analysis of Med-411FHTC and Med-2112FHTC tumorspheres treated with
631 indicated concentrations of lometrexol (LTX) for 72h (n=3). *, $P < 0.05$; **, $P < 0.01$; ***, P
632 < 0.001, Data are means ± SEM.

633 **Figure S4: Prexasertib alone has limited effect but synergizes with DHODH**
634 **inhibition.** Cell proliferation analysis of HD-MB03 and Med-411FHTC tumorspheres
635 treated with increasing concentrations of **a,** prexasertib alone or **b,** brequinar in the
636 presence of indicated doses of prexasertib. Data are means ± SEM.

637 **Figure S5: JHU083+prexasertib combination limits tumor growth in vivo. a,**
638 chemical structures of DON, JHU083, and JHU395. IVIS imaging of mice orthotopically
639 implanted with **b,** HD-MB03 or **c,** Med-411FHTC -luciferase expressing tumor lines
640 treated as indicated. Images are from mid-point of treatment. Monitored weights of
641 animals from **d,** heterotopic model treated with DAU and/or prexasertib and **e,** orthotopic
642 model treated with JHU083 and/or prexasertib.

643

644 **1.** Siegel DA, Richardson LC, Henley SJ, et al. Pediatric cancer mortality and survival in the
645 United States, 2001-2016. *Cancer.* 2020; 126(19):4379-4389.
646 **2.** Juraschka K, Taylor MD. Medulloblastoma in the age of molecular subgroups: a review. *J*
647 *Neurosurg Pediatr.* 2019; 24(4):353-363.
648 **3.** Northcott PA, Shih DJ, Peacock J, et al. Subgroup-specific structural variation across 1,000
649 medulloblastoma genomes. *Nature.* 2012; 488(7409):49-56.

650 **4.** Archer TC, Ehrenberger T, Mundt F, et al. Proteomics, Post-translational Modifications, and
651 Integrative Analyses Reveal Molecular Heterogeneity within Medulloblastoma Subgroups.
652 *Cancer Cell.* 2018; 34(3):396-410.e398.
653 **5.** Conacci-Sorrell M, McFerrin L, Eisenman RN. An overview of MYC and its interactome.
654 *Cold Spring Harb Perspect Med.* 2014; 4(1):a014357.
655 **6.** Wang C, Zhang J, Yin J, et al. Alternative approaches to target Myc for cancer treatment.
656 *Signal Transduction and Targeted Therapy.* 2021; 6(1):117.
657 **7.** Dong Y, Tu R, Liu H, Qing G. Regulation of cancer cell metabolism: oncogenic MYC in the
658 driver's seat. *Signal Transduction and Targeted Therapy.* 2020; 5(1):124.
659 **8.** Pham K, Hanaford AR, Poore BA, et al. Comprehensive Metabolic Profiling of MYC-
660 Amplified Medulloblastoma Tumors Reveals Key Dependencies on Amino Acid,
661 Tricarboxylic Acid and Hexosamine Pathways. *Cancers (Basel).* 2022; 14(5).
662 **9.** Parker WB. Enzymology of purine and pyrimidine antimetabolites used in the treatment
663 of cancer. *Chem Rev.* 2009; 109(7):2880-2893.
664 **10.** Shelton J, Lu X, Hollenbaugh JA, Cho JH, Amblard F, Schinazi RF. Metabolism, Biochemical
665 Actions, and Chemical Synthesis of Anticancer Nucleosides, Nucleotides, and Base
666 Analogs. *Chem Rev.* 2016; 116(23):14379-14455.
667 **11.** Huang M, Graves LM. De novo synthesis of pyrimidine nucleotides; emerging interfaces
668 with signal transduction pathways. *Cell Mol Life Sci.* 2003; 60(2):321-336.
669 **12.** Levitzki A, Koshland DE, Jr. Cytidine triphosphate synthetase. Covalent intermediates and
670 mechanisms of action. *Biochemistry.* 1971; 10(18):3365-3371.
671 **13.** Asnagli H, Minet N, Pfeiffer C, et al. CTP Synthase 1 Is a Novel Therapeutic Target in
672 Lymphoma. *Hemasphere.* 2023; 7(4):e864.
673 **14.** Pfeiffer C, Grandits AM, Asnagli H, et al. CTPS1 is a novel therapeutic target in multiple
674 myeloma which synergizes with inhibition of CHEK1, ATR or WEE1. *Leukemia.* 2024;
675 38(1):181-192.
676 **15.** Wu F, Mao Y, Ma T, et al. CTPS1 inhibition suppresses proliferation and migration in
677 colorectal cancer cells. *Cell Cycle.* 2022; 21(24):2563-2574.
678 **16.** Durand R, Bellanger C, Kervoëlen C, et al. Selective pharmacologic targeting of CTPS1
679 shows single-agent activity and synergizes with BCL2 inhibition in aggressive mantle cell
680 lymphoma. *Haematologica.* 2024.
681 **17.** Sun Z, Zhang Z, Wang Q-Q, Liu J-L. Combined Inactivation of CTPS1 and ATR Is Synthetically
682 Lethal to MYC-Overexpressing Cancer Cells. *Cancer Research.* 2022; 82(6):1013-1024.
683 **18.** Martin E, Minet N, Boschat AC, et al. Impaired lymphocyte function and differentiation in
684 CTPS1-deficient patients result from a hypomorphic homozygous mutation. *JCI Insight.*
685 2020; 5(5).
686 **19.** Martin E, Palmic N, Sanquer S, et al. CTP synthase 1 deficiency in humans reveals its central
687 role in lymphocyte proliferation. *Nature.* 2014; 510(7504):288-292.
688 **20.** Dharia NV, Kugener G, Guenther LM, et al. A first-generation pediatric cancer dependency
689 map. *Nat Genet.* 2021; 53(4):529-538.
690 **21.** Gwynne WD, Suk Y, Custers S, et al. Cancer-selective metabolic vulnerabilities in MYC-
691 amplified medulloblastoma. *Cancer Cell.* 2022; 40(12):1488-1502.e1487.
692 **22.** O'Connor SA, Feldman HM, Arora S, et al. Neural G0: a quiescent-like state found in
693 neuroepithelial-derived cells and glioma. *Mol Syst Biol.* 2021; 17(6):e9522.

694 **23.** Weishaupt H, Johansson P, Sundström A, et al. Batch-normalization of cerebellar and
695 medulloblastoma gene expression datasets utilizing empirically defined negative control
696 genes. *Bioinformatics.* 2019; 35(18):3357-3364.
697 **24.** Cavalli FMG, Remke M, Rampasek L, et al. Intertumoral Heterogeneity within
698 Medulloblastoma Subgroups. *Cancer Cell.* 2017; 31(6):737-754.e736.
699 **25.** de Haas T, Hasselt N, Troost D, et al. Molecular risk stratification of medulloblastoma
700 patients based on immunohistochemical analysis of MYC, LDHB, and CCNB1 expression.
701 *Clin Cancer Res.* 2008; 14(13):4154-4160.
702 **26.** McPartland RP, Wang MC, Bloch A, Weinfeld H. Cytidine 5'-triphosphate synthetase as a
703 target for inhibition by the antitumor agent 3-deazauridine. *Cancer Res.* 1974;
704 34(11):3107-3111.
705 **27.** Diehl FF, Miettinen TP, Elbashir R, et al. Nucleotide imbalance decouples cell growth from
706 cell proliferation. *Nat Cell Biol.* 2022; 24(8):1252-1264.
707 **28.** Ecker J, Thatikonda V, Sigismondo G, et al. Reduced chromatin binding of MYC is a key
708 effect of HDAC inhibition in MYC amplified medulloblastoma. *Neuro Oncol.* 2021;
709 23(2):226-239.
710 **29.** Morfouace M, Shelat A, Jacus M, et al. Pemetrexed and Gemcitabine as Combination
711 Therapy for the Treatment of Group3 Medulloblastoma. *Cancer Cell.* 2014; 25(4):516-529.
712 **30.** Morrison LC, McClelland R, Aiken C, et al. Deconstruction of medulloblastoma cellular
713 heterogeneity reveals differences between the most highly invasive and self-renewing
714 phenotypes. *Neoplasia.* 2013; 15(4):384-398.
715 **31.** Costantino L, Ferrari S, Santucci M, et al. Destabilizers of the thymidylate synthase
716 homodimer accelerate its proteasomal degradation and inhibit cancer growth. *Elife.* 2022;
717 11.
718 **32.** Guijarro MV, Kellish PC, Dib PE, et al. First-in-class multifunctional TYMS nonclassical
719 antifolate inhibitor with potent in vivo activity that prolongs survival. *JCI Insight.* 2023;
720 8(10).
721 **33.** Schild T, Keshari KR. Revealing de novo pyrimidine synthesis as a key vulnerability in brain
722 tumors. *Cancer Cell.* 2022; 40(12):1457-1458.
723 **34.** Endersby R, Whitehouse J, Pribnow A, et al. Small-molecule screen reveals synergy of cell
724 cycle checkpoint kinase inhibitors with DNA-damaging chemotherapies in
725 medulloblastoma. *Science Translational Medicine.* 2021; 13(577):eaba7401.
726 **35.** Ianevski A, Giri AK, Aittokallio T. SynergyFinder 3.0: an interactive analysis and consensus
727 interpretation of multi-drug synergies across multiple samples. *Nucleic Acids Research.*
728 2022; 50(W1):W739-W743.
729 **36.** Stewart DJ, Benvenuto JA, Leavens M, et al. Penetration of 3-Deazauridine into Human
730 Brain, Intracerebral Tumor, and Cerebrospinal Fluid1. *Cancer Research.* 1979;
731 39(10):4119-4122.
732 **37.** Hirano A, Matsui T. Vascular structures in brain tumors. *Hum Pathol.* 1975; 6(5):611-621.
733 **38.** Phoenix TN, Patmore DM, Boop S, et al. Medulloblastoma Genotype Dictates Blood Brain
734 Barrier Phenotype. *Cancer Cell.* 2016; 29(4):508-522.
735 **39.** Weng ML, Zalkin H. Structural role for a conserved region in the CTP synthetase glutamine
736 amide transfer domain. *J Bacteriol.* 1987; 169(7):3023-3028.

40. Ortlund E, Lacount MW, Lewinski K, Lebioda L. Reactions of Pseudomonas 7A glutaminase-asparaginase with diazo analogues of glutamine and asparagine result in unexpected covalent inhibitions and suggests an unusual catalytic triad Thr-Tyr-Glu. *Biochemistry.* 2000; 39(6):1199-1204.

41. Pham K, Maxwell MJ, Sweeney H, et al. Novel Glutamine Antagonist JHU395 Suppresses MYC-Driven Medulloblastoma Growth and Induces Apoptosis. *J Neuropathol Exp Neurol.* 2021; 80(4):336-344.

42. Hanaford AR, Alt J, Rais R, et al. Orally bioavailable glutamine antagonist prodrug JHU-083 penetrates mouse brain and suppresses the growth of MYC-driven medulloblastoma. *Transl Oncol.* 2019; 12(10):1314-1322.

43. Campagne O, Davis A, Maharaj AR, et al. CNS penetration and pharmacodynamics of the CHK1 inhibitor prexasertib in a mouse Group 3 medulloblastoma model. *Eur J Pharm Sci.* 2020; 142:105106.

44. Minet N, Boschat AC, Lane R, et al. Differential roles of CTP synthetases CTPS1 and CTPS2 in cell proliferation. *Life Sci Alliance.* 2023; 6(9).

45. Mariotto E, Rampazzo E, Bortolozzi R, et al. Molecular and functional profiling of chemotolerant cells unveils nucleoside metabolism-dependent vulnerabilities in medulloblastoma. *Acta Neuropathol Commun.* 2023; 11(1):183.

46. Lemberg KM, Vornov JJ, Rais R, Slusher BS. We're Not "DON" Yet: Optimal Dosing and Prodrug Delivery of 6-Diazo-5-oxo-L-norleucine. *Mol Cancer Ther.* 2018; 17(9):1824-1832.

47. Nedelcovych MT, Tenora L, Kim BH, et al. N-(Pivaloyloxy)alkoxy-carbonyl Prodrugs of the Glutamine Antagonist 6-Diazo-5-oxo-l-norleucine (DON) as a Potential Treatment for HIV Associated Neurocognitive Disorders. *J Med Chem.* 2017; 60(16):7186-7198.

48. Rais R, Jančařík A, Tenora L, et al. Discovery of 6-Diazo-5-oxo-l-norleucine (DON) Prodrugs with Enhanced CSF Delivery in Monkeys: A Potential Treatment for Glioblastoma. *J Med Chem.* 2016; 59(18):8621-8633.

49. Lee K, Thompson EA, Gharaie S, et al. T cell metabolic reprogramming in acute kidney injury and protection by glutamine blockade. *JCI Insight.* 2023; 8(12).

50. Praharaj M, Shen F, Lee AJ, et al. Metabolic reprogramming of tumor-associated macrophages using glutamine antagonist JHU083 drives tumor immunity in myeloid-rich prostate and bladder cancer tumors. *Cancer Immunol Res.* 2024.

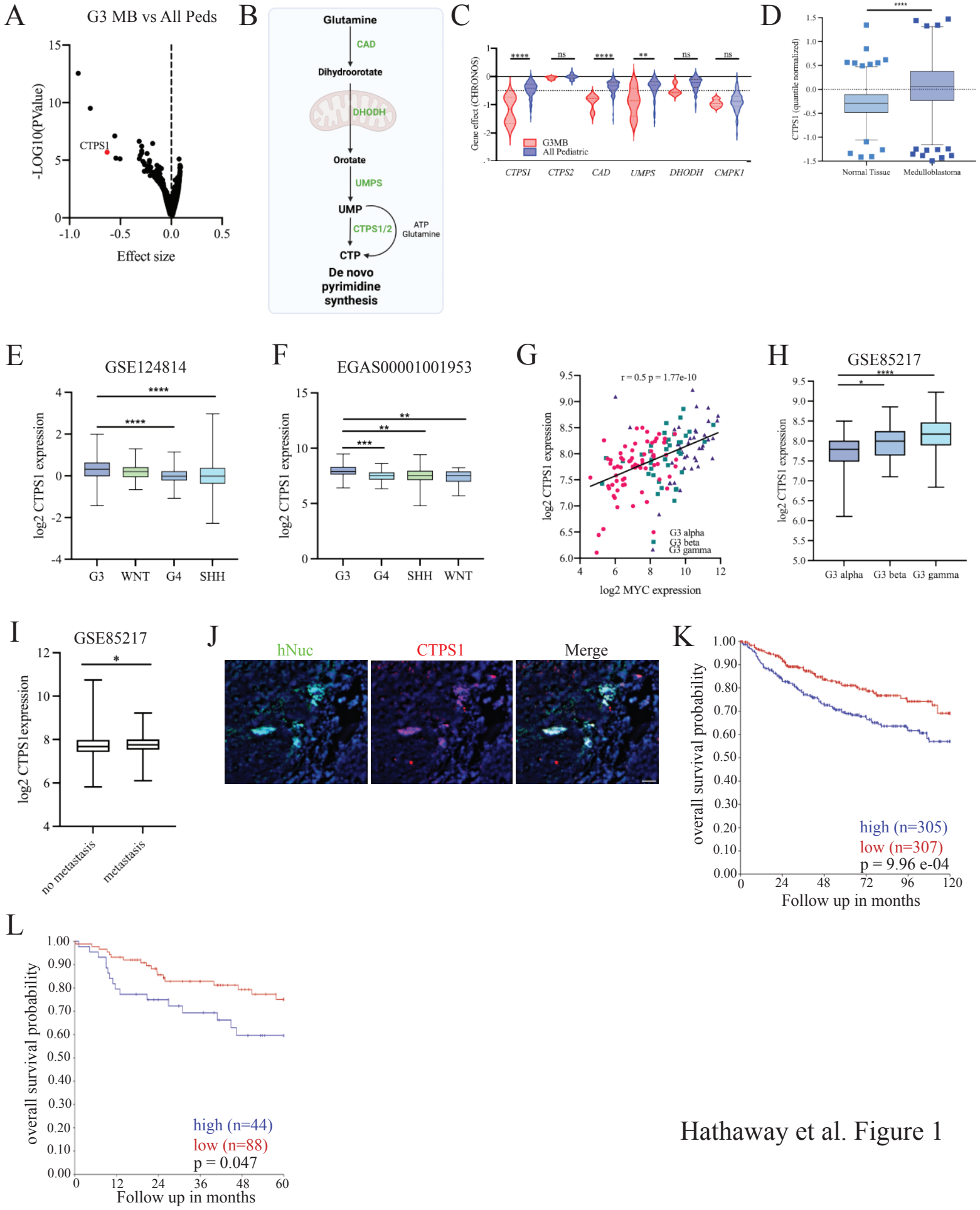

Hathaway et al. Figure 1

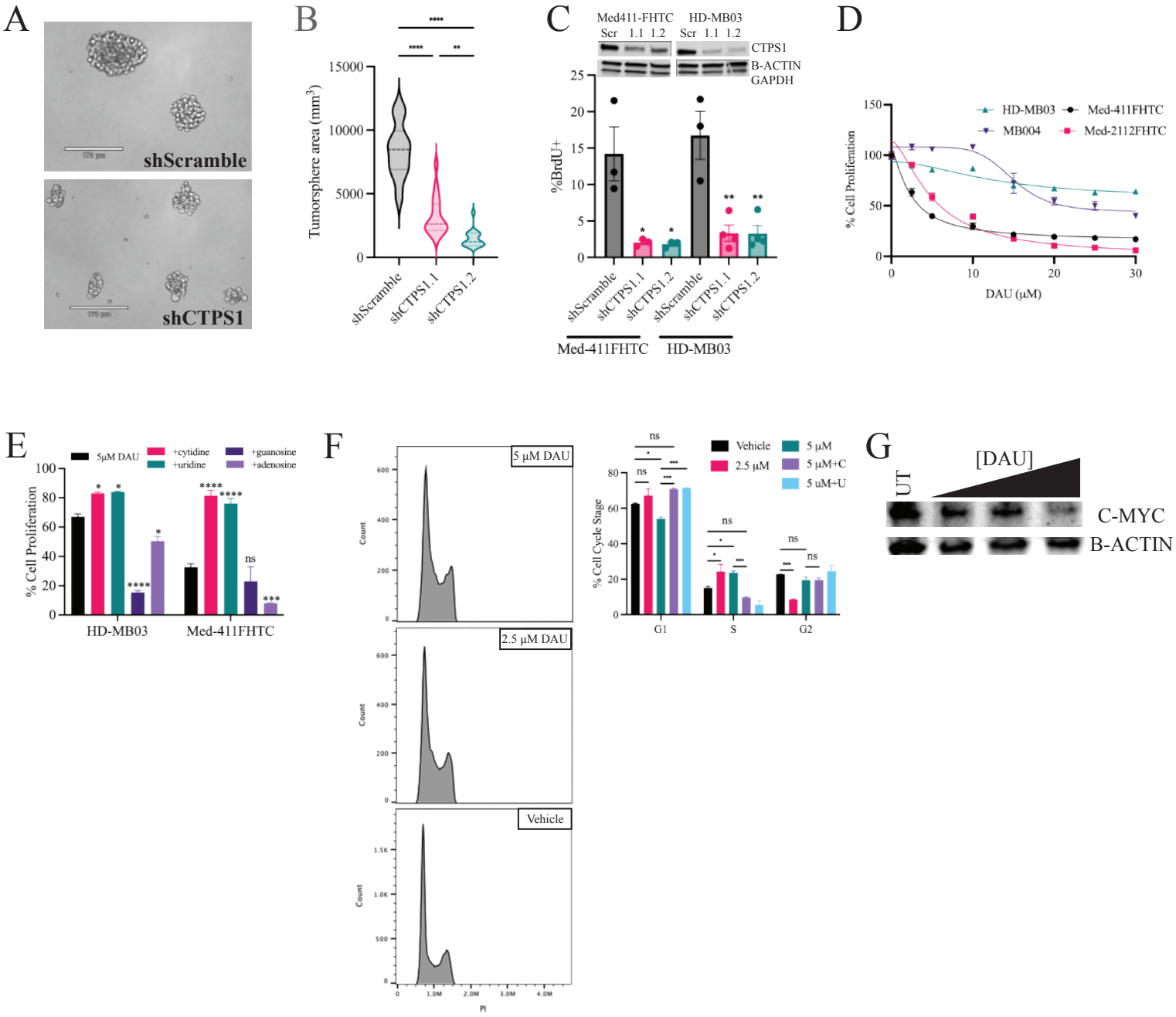

Hathaway et al. Figure 2

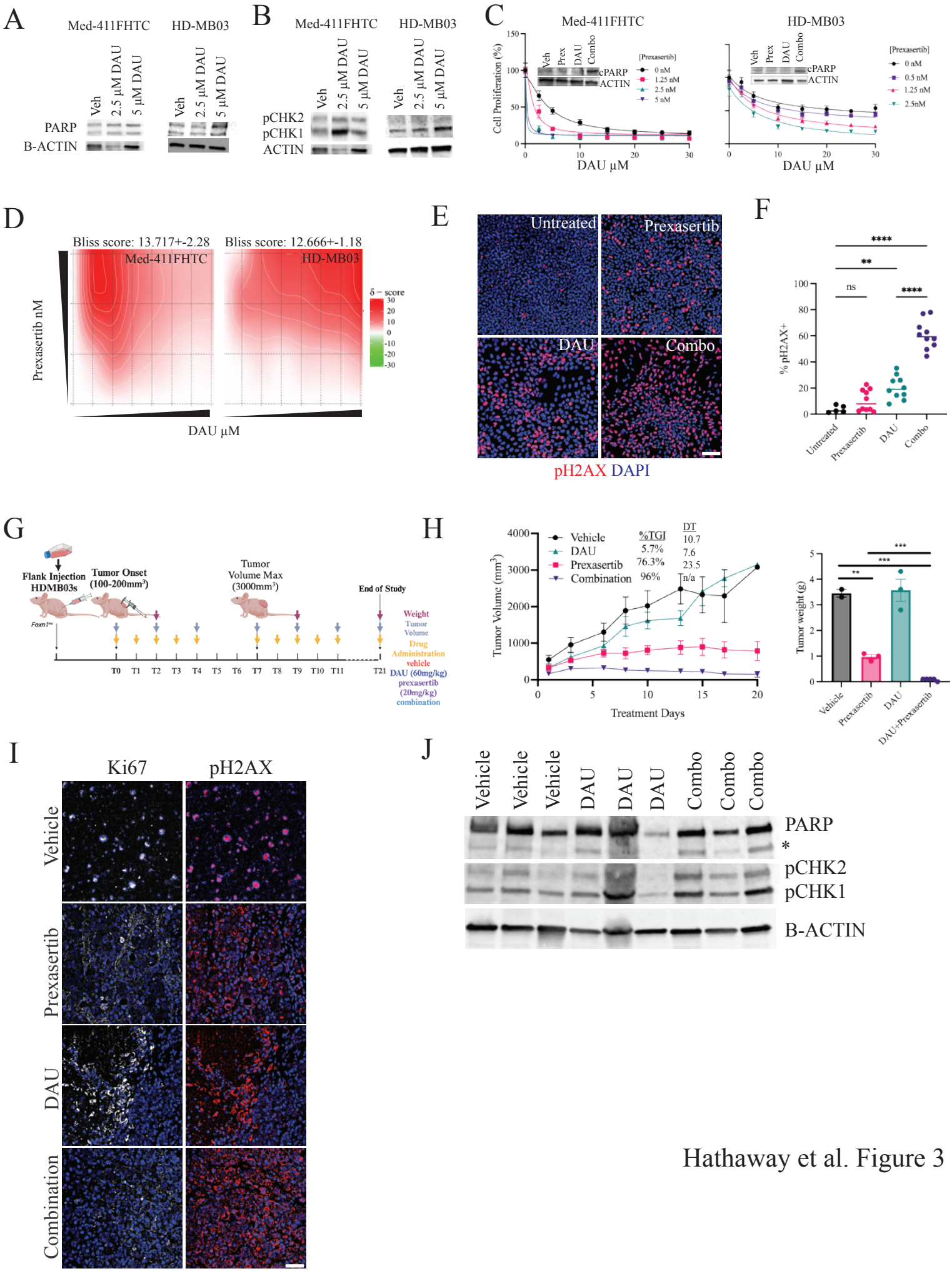

Hathaway et al. Figure 3

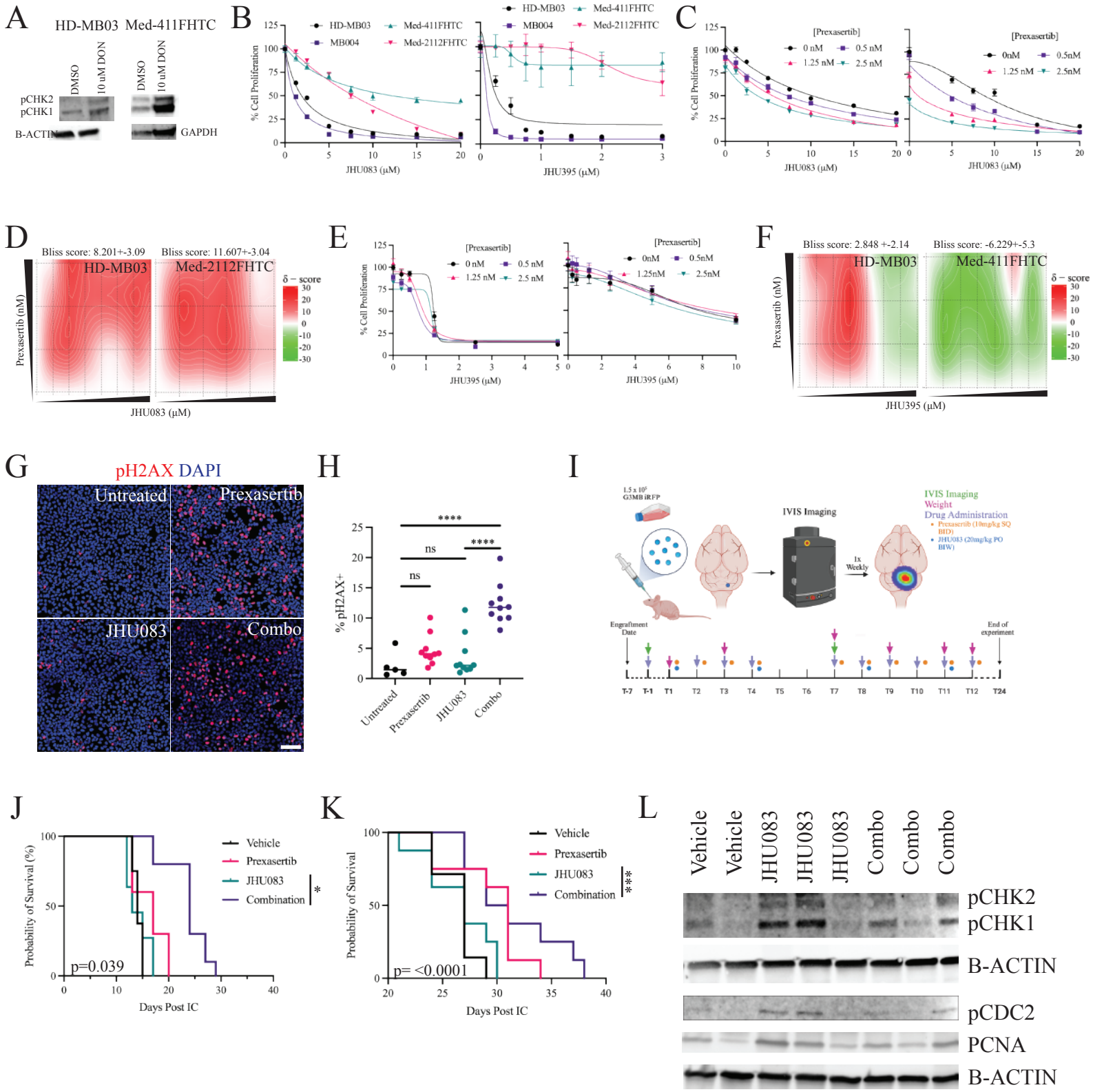

Hathaway et al. Figure 4

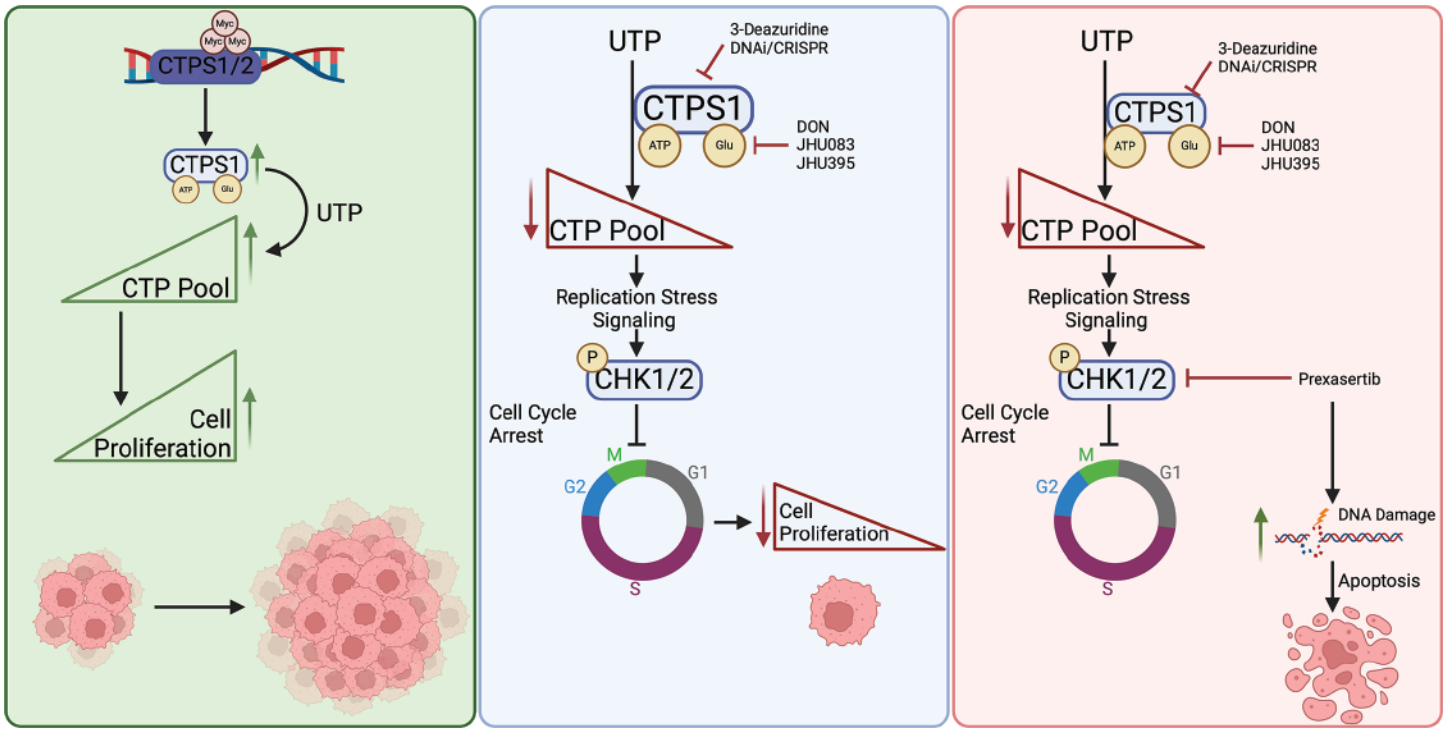

Hathaway et al. Figure 5

Table 1: Synergy scores for CTPS1 inhibitiors with prexasertib

	Drug 1	Drug 2	ZIP_synergy	ZIP_synergy_p_value	HSA_synergy	HSA_synergy_p_value	Loewe_synergy	Loewe_synergy_p_value	Bliss_synergy	Bliss_synergy_p_value
HD-MB03	prexasertib	DAU	12.60639662	5.33E-20	17.40683667	3E-117	10.83592936	0.000055	12.0364247	6.25E-15
	prexasertib	JHU395	5.489365734	0.000469	8.794607635	2.34E-08	-1.769786284	0.886	5.237058489	0.00347
	prexasertib	JHU083	6.122734406	0.0211	12.55551008	8.69E-21	9.364874489	0.000188	5.965281089	0.027
Med-411FHTC	prexasertib	DAU	11.03533493	4.03E-19	13.89670691	2.03E-92	8.049172603	0.101	10.78442356	2.35E-14
	prexasertib	JHU395	-1.533340467	0.655	-4.356167358	0.0353	-7.164625504	0.172	-3.25086577	0.396
	prexasertib	JHU083	8.805722263	0.0000897	18.33827545	6.16E-18	4.763895713	0.534	8.852162691	0.0000665